

Article

Analysis of Electrical Models for Photovoltaic Cells under Uniform and Partial Shading Conditions

Bonie Johana Restrepo-Cuestas ^{1,*}, Mariana Durango-Flórez ^{1,†}, Luz Adriana Trejos-Grisales ^{1,†}
and Carlos Andrés Ramos-Paja ^{2,†}

¹ Facultad de Ingenierías, Instituto Tecnológico Metropolitano, Medellín 050028, Colombia; marianadurango5032@correo.itm.edu.co (M.D.-F.); adrianatrejos@itm.edu.co (L.A.T.-G.)

² Facultad de Minas, Universidad Nacional de Colombia, Medellín 050034, Colombia; caramosp@unal.edu.co

* Correspondence: bonierestrepo@itm.edu.co

† These authors contributed equally to this work.

Abstract: This paper compares the performance of three electrical models (the single diode model, the Bishop model, and the Direct-Reverse model) in representing photovoltaic cells. Such comparison is performed in both the first quadrant (positive cell voltage and current— Q_1) and the second quadrant (negative cell voltage and positive cell current— Q_2). The analysis conducted here is based on the I–V curves of a PV cell obtained experimentally. The parameters of each model are estimated using a Genetic Algorithm. The root mean square error and the mean absolute percentage error are computed to validate the estimation stage. Likewise, the behavior of each parameter of the models is analyzed by calculating their mean and standard deviation. Some places of interest on the I–V curve, such as the short-circuit point, the open-circuit point, and the maximum power point, are also estimated and compared.

Keywords: photovoltaic cell; single diode model (SDM); the Bishop model; Direct-Reverse model (DRM); genetic algorithm (GA)



Citation: Restrepo-Cuestas, B.J.; Durango-Flórez, M.; Trejos-Grisales, L.A.; Ramos-Paja, C.A. Analysis of Electrical Models for Photovoltaic Cells under Uniform and Partial Shading Conditions. *Computation* **2022**, *10*, 111. <https://doi.org/10.3390/computation10070111>

Received: 19 May 2022

Accepted: 6 June 2022

Published: 30 June 2022

Publisher's Note: MDPI stays neutral with regard to jurisdictional claims in published maps and institutional affiliations.



Copyright: © 2022 by the authors. Licensee MDPI, Basel, Switzerland. This article is an open access article distributed under the terms and conditions of the Creative Commons Attribution (CC BY) license (<https://creativecommons.org/licenses/by/4.0/>).

1. Introduction

Photovoltaic (PV) systems are a cost-effective option to face the world's recent environmental and energy challenges. In 2020, installed PV capacity reached 107 GW, and this figure is expected to keep on increasing by an average of 125 GW between 2021 and 2025 [1]. The rapid expansion of such systems requires paying special attention to the development of tools that are able to analyze and predict the behavior of PV sources in order to design suitable sizing and planning strategies.

When analyzing the behavior of PV arrays, aspects such as power generation, shading impact, Maximum Power Point Tracking (MPPT) controller design [2], and degradation are examined. However, power generation is one of the most important aspects because it is associated with performance and reliability. The power output in PV systems is mainly affected by partial shading, a condition that forces the shaded cells to consume power rather than produce it [3]. This condition imposes a negative voltage on its terminals, making the cell operate in the second quadrant Q_2 (negative cell voltage and positive cell current, thus consuming power). Figure 1 shows the experimental I–V curve of a monocrystalline cell with short-circuit current $I_{sc} = 0.43$ A and open-circuit voltage $V_{oc} = 0.5$ V. Such a figure shows both the first and second quadrants Q_1 and Q_2 , respectively, where Q_1 exhibits positive cell voltage and current, hence producing power. Finally, the operation of the cell in Q_2 is also known as reverse mode.

The first step in performing a proper analysis of PV arrays is to represent the operation of the PV cells and modules using circuit models such as the Single Diode Model (SDM), which is widely used due to its tradeoff between complexity and accuracy [4], or the Double Diode Model (DDM), which is more accurate to represent the p–n junction at low

irradiance levels [5]. The Bishop model [6], for its part, aims to represent the behavior of a PV cell operating under partial shading conditions, which requires considering the second quadrant (Q_2). Another model designed to study the behavior of PV cells under partial shading conditions is the Direct Reverse Model (DRM). This model is able to reproduce the operation of cells in either direct or reverse biasing modes to account for the influence of variations in temperature and solar irradiance [7].

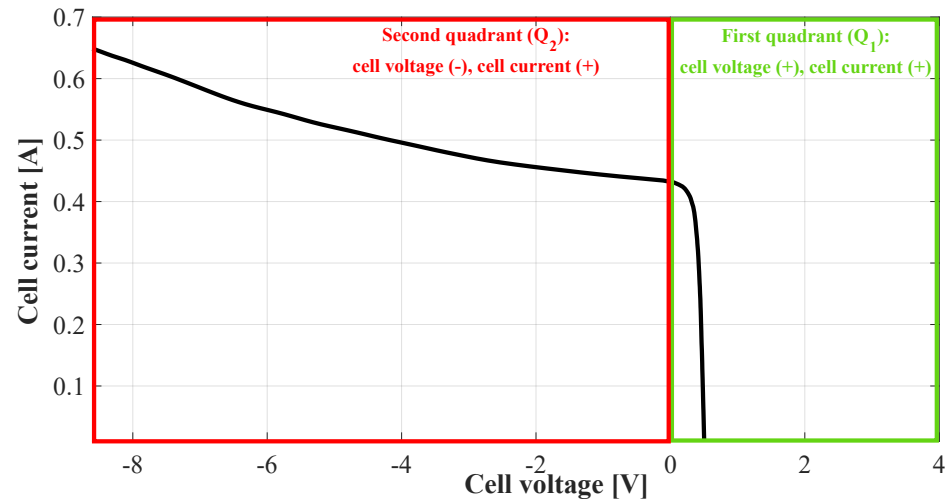


Figure 1. The electrical characteristic of a PV cell.

The previous mathematical models require the accurate identification of a set of parameters to obtain a high-performance in the reproduction of the cell behavior. Several parameter estimation techniques have been reported in the literature for the different PV cell models. Those techniques can be divided into three categories: analytical, metaheuristic and hybrid techniques [8]. Each of these techniques require some initial data, which can be obtained from the manufacturer's datasheet or from experimental tests.

Analytical techniques use a series of mathematical equations for parameter extraction, which, in some cases, can result in a high computational burden and complex mathematical operations, which increases the computational time [8]. Metaheuristic techniques define the parameter identification problem as an optimization problem [4]. These are a promising alternative because they do not require an accurate mathematical model; instead, they need an objective function and a parameter search range, which can be more effective and less time consuming. Furthermore, those techniques evolve several individuals for the problem, which reduces the procedure's sensitivity to the initial guess and provides a strong ability to jump out of a local optima [8]. Finally, hybrid techniques extract some of the initial parameters using analytical approaches, while the rest of the parameters are estimated by means of optimization algorithms.

Recent publications on the parameter estimation problem suggest that metaheuristics methods have become a relevant research area for all PV circuit models. For instance, the Slime Mold Algorithm (SMA) [9], the Grasshopper Optimization Algorithm (GOA) [10], Principal Component Analysis (PCA) [11], Particle Swarm Optimization (PSO) [12], Triple-Phase Teaching-Learning-Based Optimization (TPTLBO) [13], and Perturbed Stochastic Fractal Search (pSFS) [14] have been used to extract the parameters of the SDM. For DDM, some of the solutions that have been adopted include the moth flame optimization [15], improved differential evolutionary algorithm [16], the Pattern Search (PS) algorithm [5], the Crow Search Algorithm [17], and the Wind-Driven Optimization (WDO) algorithm [18]. However, Genetic Algorithms (GA) are the most widely adopted solution for the parameter estimation in PV systems. For example, the work reported in [19] proposes a new variant of the GA, which integrates a new crossover operation to maintain a good balance between the intensification of the best solutions and the diversification of the search space; such a

solution was designed to identify the electrical parameters of different PV cell models (SDM and DDM). Similarly, in [20] the authors extract the solar cell parameters for a Kyocera panel (KC200GT) using GA. In [21], an inverse modeling method for PV panel is proposed, which is based on parameter identification through GA. Such a process generates random groups of 5 parameters which are entered into the SDM; then, the parameters that generate a power output most similar to the experimental value are selected. On the other hand, ref. [22] proposes an algorithm for datasheet parameter extraction of photovoltaic modules using the SDM, where the extracted parameters are obtained by approximation using a GA. Authors in [23] present the implementation of a continuous population genetic optimization algorithm (CGA) as a solution method for the parameter estimation of the diode model (SDM) in a PV panel from experimental data. Such a procedure was validated with four different panels: Solarex MSX60, SOLAR SJ65, KYOCERA KC200GT, and STP245S.

Although the Bishop model is one of the most cited and used models to represent a PV cell operating under partial shading conditions [3,24–26], there is not a clear procedure to estimate its parameters; instead, authors typically use parameters already reported in the literature. A similar situation occurs for the DRM [27]. Given the importance of having an accurate model for PV power generation analysis under partial shading conditions, there is a need for procedures to identify the parameters of the models. Moreover, procedures with a good relationship between complexity and accuracy, and the ability to be applied for different PV models, are also needed.

Therefore, this paper presents a behavior comparison between three models (SDM, Bishop, DRM) when the estimation of the current vs. voltage (I–V) curve in both Q_1 and Q_2 is needed. For this analysis, the first stage consists in estimating the parameters of the SDM, the Bishop model, and the DRM using genetic algorithms and Simulink simulations. Thus, the parameters to be estimated, the objective function, and the set of restrictions considered in the mathematical formulation for each model, are proposed. This study was validated by comparing two error measures (RMSE and MAPE) obtained from the I–V curve reconstruction of an experimental PV cell for each model, i.e., in both the first (Q_1) and second (Q_2) quadrants. Also, the result of the estimation of some points of interest, such as short-circuit current (I_{sc}), open-circuit voltage (V_{oc}), and voltage and current at the maximum power point (V_{mpp} , I_{mpp}) were evaluated and analyzed for each model. Finally, this work provides an estimation guide for modeling the behavior in the first and second quadrants, which is essential for evaluating power losses in photovoltaic systems under partial shadowing.

The rest of this paper is structured as follows. Section 2 presents the main characteristics of the models. Section 3 describes the parameter estimation proposed here, which adopts the GA and Simulink simulations. Section 4 discusses the results of the proposed parameter estimation procedure. Finally, Section 5 draws the conclusions of the research.

2. Methods

This section describes the models' mathematical representation, highlighting the parameters to be estimated.

2.1. Single Diode Model

The Single Diode Model (SDM), also known as the five-parameter model, is represented by the equivalent circuit in Figure 2. In this circuit the current source is associated with the PV current and, the diode represents the energy level threshold for photons to trigger significant production and circulation of electron-hole pairs through the junction [28]. Losses are represented by a series resistance (R_s), which is related to the metal–semiconductor contact resistance, the ohmic resistance of the contacts, and the ohmic resistance of the semiconductor material. The leakage currents along the edges of the cell are represented by shunt resistor (R_{sh}).

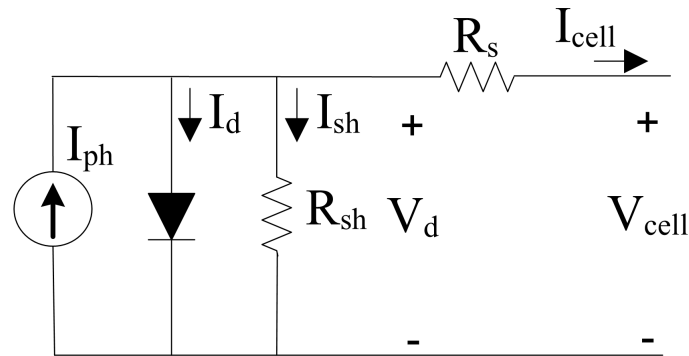


Figure 2. Circuit diagram of the Single Diode Model.

The cell current (I_{cell}) be obtained as the algebraic sum of the currents through the diode (I_d), the current through the shunt resistor (I_{sh}) and the photocurrent (I_{ph}). Shockley’s equation [29] models the current–voltage relationship in the diode ($I_d - V_d$). Thus, (1) represents the resulting cell current (I_{cell}).

$$I_{cell} = I_{ph} - I_0 \left(e^{(V_{cell} + I_{cell}R_s) / AV_T} - 1 \right) - \frac{(V_{cell} + I_{cell} * R_s)}{R_{sh}} \tag{1}$$

In Equation (1), V_{cell} is the cell voltage; and I_0 and A , the reverse saturation current and the ideality factor of the diode, respectively. Finally, V_T represents the thermal potential expressed in Equation (2), where k is the Boltzmann constant; T , the temperature of the cell; and q , the electron charge.

$$V_T = kT/q \tag{2}$$

According to the previous equations, five parameters (R_s , R_{sh} , I_{ph} , I_0 , and A) must be evaluated in the SDM to obtain the I–V characteristics of a PV cell. Importantly, this model is only used to represent the behavior of PV cell in Q_1 when is delivering energy.

2.2. The Bishop Model

The model proposed by Bishop incorporates an avalanche mechanism into the SDM. As depicted in Figure 3, this mechanism represents the reverse characteristics of the PV cell, which is controlled by the current through R_{sh} . This current term is composed of an ohmic term and a nonlinear multiplication factor [6] as shown in Equation (3).

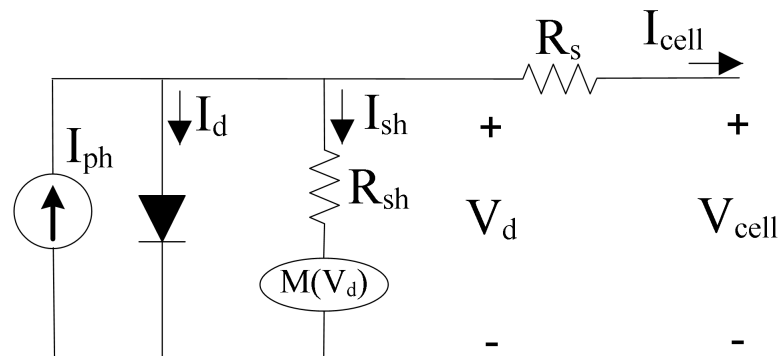


Figure 3. Circuit diagram of the Bishop Model.

In the Bishop model, Equation (3) relates the output current and the voltage of a PV cell, where a is the ohmic fraction of the current related to the avalanche breakdown; m , the avalanche breakdown exponent; and V_{br} , the junction breakdown voltage.

$$I_{cell} = I_{ph} - I_0 \left(e^{\frac{(V_{cell} + I_{cell}R_s)}{AV_T}} - 1 \right) - \frac{(V_{cell} + I_{cell} * R_s)}{R_{sh}} \left(1 + a * \frac{(1 - (V_{cell} + I_{cell}R_s))}{V_{br}} \right)^{-m} \tag{3}$$

To represent the Bishop model, eight parameters ($R_s, R_{sh}, I_{ph}, I_0, A, V_{br}, m, a$) must be estimated. This model is commonly used to represent the behavior of a PV cell in both Q_1 and Q_2 , with the cell consuming instead of producing power in Q_2 .

2.3. Direct–Reverse Model

The Direct–Reverse Model (DRM) makes it possible to model the behavior of PV cells in both direct and reverse polarization modes. Using the I–V characteristics from the same sorted series cells, the authors of [27,30,31] studied the variability of the curves, not only in the value of the breakdown voltage but also in the slopes of the ohmic regions in Q_2 . Based on this characterization, they were able to observe parts of the curve in Q_2 that could be linearized. In this model, a Thevenin equivalent in series with a diode in the opposite mode models each linear part, where the Thevenin resistance represents the slope of the linear region. As shown in Figure 4, this model evaluates the behavior of a PV cell in Q_1 using the double–diode model.

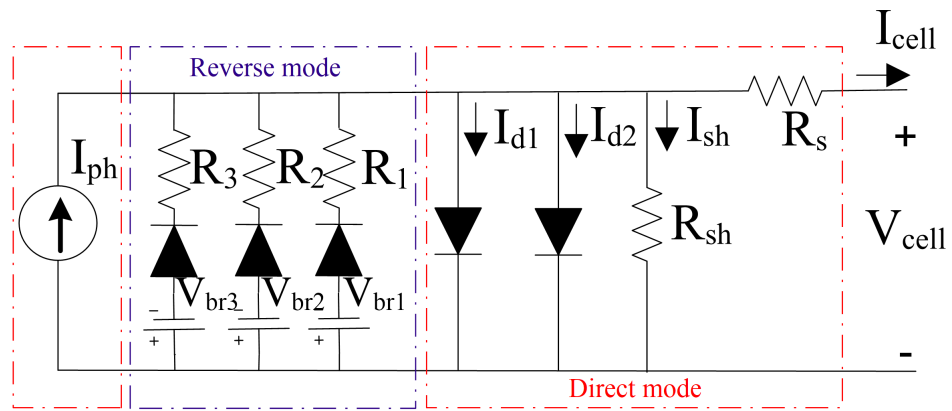


Figure 4. Circuit diagram of the Direct-Reverse Model.

The number of PV parameters that must be estimated depends on the number of branches used to represent the linear approximation. In the example of Figure 4, the circuit is represented by 13 parameters (7 for the direct mode and 6 for the reverse mode). The DRM can be used for both Q_1 and Q_2 representation.

2.4. PV Panel/Array Modeling

An important application of the models described above lies in the capacity of been employed for the PV panel/array modeling, in both Q_1 and Q_2 . PV panel modeling is based on the PV cell model and the number of cells connected in series (N_s) and in parallel (N_p), as shown in Equation (4). Therefore, when modeling a PV array modeling, the number of panels and their connection must be considered. Another key aspect is the procedure used to solve the resulting equations regarding the connection between the PV panels and the number of parameters to estimate. The I–V characteristics of a PV array, as well as the maximum power reached under a given operating condition, can be obtained by solving such equations.

$$I_M = N_p * I_{ph} - N_p * I_0 * \left(e^{\frac{V_M + I_M * \frac{N_s}{N_p} * R_s}{AV_T}} - 1 \right) - \frac{V_M + I_M * \frac{N_s}{N_p} * R_s}{\frac{N_s}{N_p} * R_{sh}} \tag{4}$$

As previously discussed, each PV model has a defined number of parameters to estimate. Also, due to the nonlinear current–voltage relationship of the models, the cell or panel current (I) is expressed as an implicit function of its voltage (V), i.e., $f(I, V) = 0$, which requires the use of numerical methods for its analysis and solution. Three types of techniques for parameter estimation have been reported in the literature: (i) metaheuristic

techniques such as GA; (ii) analytical techniques such as Lambert W and iterative methods like the Newton–Raphson method; and (iii) hybrid techniques, which use metaheuristic and analytical methods for a more accurate I–V representation. Regarding the SDM, the authors of [32] used a Differential Evolution (DE) algorithm to estimate its five parameters, while the authors of [33] employ a Hybrid Java–NM algorithm for parameter extraction. The Newton–Raphson method was used in [34], whereas the Lambert W function was employed in [35] to find a solution. Due to its low complexity, the SDM is the most commonly used model for PV array modeling, as highlighted by the authors of [36]. Studies such as that in [37] suggest that parameter estimation for SDM and the DDM, which is an extension of the SDM [38], can be estimated using the same algorithm. As a result, similar computational times are obtained depending on the technique used. In the case of metaheuristic algorithms, the objective function employed, and the tuning parameters of the algorithm have a considerable impact on computational times. The Bishop model can be enhanced with the SDM and the DDM. For instance, authors of [39] modeled a PV array employing the Bishop model with double diode. This solution, nonetheless, may require a higher computational time and be more complex due to the number of variables to estimate. In [40], the Bishop model was used for PV panel modeling, and each PV panel, string, and array were modeled using a piecewise polynomial function approximation, a process similar to that of the DRM. The DRM, which is similar to the Bishop model, is employed to model a PV cell behavior in both the direct and reverse operating modes. Nevertheless, the number of parameters to estimate, which is associated with the number of branches used to model the PV cell, makes it a complex model for PV parameter estimation and PV array modeling. Despite this, authors of [24] used the DRM to model a PV string. In addition, considering the PV panels connected in series/parallel, this model can be used for PV array representation. The complexity in modeling a PV array is determined by the PV cell model used. Therefore, depending on the PV cell data available, such as its technology (e.g., polycrystalline and CIGS), I–V characteristics, and working zone of the experimental tests (e.g., Q_1), the PV models discussed above can be employed for such purpose considering the number of variables to estimate and the method used to solve the associated equations. This study provides a first stage procedure for choosing a proper PV model for a given working condition by comparing the performance of each model with experimental data obtained from a PV cell.

3. Proposed Parameter Estimation Technique

The parameter estimation problem for each model presented in Section 2 was solved using the GA. Each step of the estimation process, which are explained in the next subsections, are related to the fitness function and the search space constrains, both of which must be accurately defined to avoid falling into a local minimum. A set of constrains, determined by the search space of the parameters when modeling PV cells, must also be defined. The literature describes the search space for the SDM and DDM of PV cells [41,42] to represent only Q_1 . Those ranges can be applied to the parameters that are shared by the Bishop model and the DRM; however, search ranges for the parameters that determine the behavior of PV cells in Q_2 are also required. In the DRM, these ranges can be obtained using information contained in the experimental data of the I–V curve.

3.1. Initial Population

A set of solution vectors is randomly generated within the search space to establish the current population, whose size is denoted by the population size (p). All solution vectors in the initial population must be different (diversity criterion). Then, the fitness function of each solution vector is evaluated, and that with the minimum value is selected as the incumbent.

3.2. Selection

Chosen randomly from the initial population, with a length given by a random integer (r). Therefore, to complete the new population, $r-p$ solution vectors must be created. Next, a pair of solution vectors, which are named parents, are selected to proceed to the crossover stage.

3.3. Crossover

In this stage, the two solution vectors selected are combined to produce a new vector called offspring, for which a parent crossing point is chosen. Thus, offspring will carry information from both parents.

3.4. Mutation

This operation produces spontaneous changes in offspring. It is a random alteration of the value at an offspring's position.

3.5. Population Update

The algorithm repeats the selection, crossover, and mutation processes until p children are created. The fitness function of the offspring population must also be evaluated. Offspring and the initial population are concatenated, and then sorted in ascending order based on the evaluation of their fitness function. The first best p solution vectors will be selected as the initial population of the next generation.

3.6. Stopping Criterion

In this study, the stop criterion is the maximum number of iterations for the estimation process ($itermax$), which are referred to as generations. Algorithm 1 presents the pseudocode of the GA described above.

Algorithm 1: Pseudocode of GA applied to PV cell parameter estimation.

Data: Experimental $I - V$ data, p , $itermax$, search ranges
Result: φ

```

1 iter=1;
2 Generate initial population;
3 Evaluate the fitness function and constrains;
4 Select the best solution;
5 while iter = 2 : itermax do
6   for i = 1 : p do
7     Select r vectors of initial population;
8     Create r-p vectors randomly;
9     Generate the new population combining selected and created vectors;
10    Select two parents randomly from the new population;
11    Create offspring by recombining parents;
12    Mutate offspring;
13    Select the best offspring;
14  end
15  Generate offspring population;
16  Evaluate fitness function and constrains;
17  New population= [initial population; offspring population];
18  Initial population= the best p solution vectors;
19  Select the best solution  $\varphi$ ;
20 end

```

3.7. Fitness Function

The fitness function (*FF*) of the optimization problem addressed in this study, is to minimize the root mean square error (*RMSE*) between the cell current measured in the experimental tests (I_{cell_m}) and the value estimated with the optimization technique ($I_{cell_e}(\phi)$), as shown in Equation (5).

$$\min[FF(\phi)] = \min[RMSE(I_{cell_e}(\phi), I_{cell_m})] = \min \left[\sqrt{\frac{1}{N} \sum_{i=1}^N (I_{cell_e}(\phi) - I_{cell_m})^2} \right] \quad (5)$$

$I_{cell_e}(\phi)$ results from evaluating the implicit Equations (1) and (3) using the Newton Raphson method and the estimated parameters. ϕ is the solution vector, which includes the unknown parameters of the model to be identified and N is the number of samples. Table 1 presents the coding for the optimization problem considered here, which, as stated in the previous section, depends on the adopted PV model since each model has a specific number of parameters that describe its I–V characteristics.

Table 1. Evaluation of the estimated I_{cell} for each model.

Model	$I_{cell_e}(\phi)$	Parameters to Estimate (ϕ)	Operation Mode
SDM	(1)	$[I_{ph}, I_0, A, R_s, R_{sh}]$	Q_1
Bishop	(3)	$[I_{ph}, I_0, A, R_s, R_{sh}, V_{br}, m, a]$	Q_1, Q_2
DRM	(1) Only for Q_1	$[I_{ph}, I_0, A, R_s, R_{sh}]$	Q_1, Q_2

3.8. Problem Constrains

The constraints of the optimization problem correspond to the search ranges of the parameters to be estimated, which are defined in Equations (6)–(13). Those parameters correspond to the models reported in Section 2, where the search ranges should be respected to ensure a correct estimation of the parameters in each model as presented in Table 2.

$$A_{min} \leq A \leq A_{max} \quad (6)$$

$$R_{smin} \leq R_s \leq R_{smax} \quad (7)$$

$$R_{shmin} \leq R_{sh} \leq R_{shmax} \quad (8)$$

$$I_{omin} \leq I_o \leq I_{omax} \quad (9)$$

$$I_{phmin} \leq I_{ph} \leq I_{phmax} \quad (10)$$

$$a_{min} \leq a \leq a_{max} \quad (11)$$

$$m_{min} \leq m \leq m_{max} \quad (12)$$

$$V_{brmin} \leq V_{br} \leq V_{brmax} \quad (13)$$

Table 2. Number of constraints for each model.

Model	Constrains
SDM	Equations (6)–(10)
Bishop	Equations (6)–(13)
DRM	Equations (6)–(10)

4. Results and Discussion

The I–V curve for the validation process was obtained from a monocrystalline cell with the following electrical characteristics, which was exposed to an irradiance of 1008 W/m² and a temperature of 47.8 °C:

- Short-circuit current $I_{sc} = 0.43$ A
- Open-circuit voltage $V_{oc} = 0.5$ V

- Maximum power current $I_{mp} = 0.36$ A
- Maximum power voltage $V_{mp} = 0.5$ V

The models were simulated in MATLAB® R2021a on a computer with an Intel Core i5–5200U 2.2 GHz processor, 8 GB of RAM, and Windows 10 pro. The results obtained with each model, which are presented in the next subsection, were contrasted with the I–V curve obtained experimentally. Table 3 reports the values of the constraints (i.e., the range of the parameters) used for the estimation problem addressed in this study.

Table 3. Parameter constraints.

Parameter	Minimum Value	Maximum Value
I_{ph}	90% * I_{ph} [A]	110% * I_{ph} [A]
I_0	1×10^{-10} [A]	1×10^{-7} [A]
A	0.05	4
R_s	1×10^{-5} [Ω]	2 [Ω]
R_{sh}	20 [Ω]	100 [Ω]
V_{br}	–10 [V]	–50 [V]
m	2	8
a	1×10^{-3}	30×10^{-3}

The number of individuals per population and the maximum number of iterations were defined by evaluating the GA in a range of [5, 70] individuals per population and [500, 5000] iterations. Figure 5 illustrates the tuning results for the SDM. As observed in Figure 5a, there is an increment in the number of individuals per population and a decrement in the average value of the objective function with a decreasing number of iterations. Figure 5b shows the contour of the surface, which reports that the objective function reaches its minimum value with 65 individuals and after 1500 iterations. A parameter tuning was performed to determine the best number of individuals and iterations for estimating the parameters of each model. Table 4 shows the results of that tuning process.

Table 4. Selection of GA variables for each model.

Variable	Individual per Population	Number of Iterations
SDM	60	1500
Bishop	5	500
DRM	60	500

Then, 100 repetitions of the parameter estimation algorithm (Algorithm 1) were evaluated using the GA variables provided in Table 4 for each model, where the mean and standard deviation of each estimated parameter of the SDM, Bishop model, and DRM were calculated. Those metrics were also computed for the root mean square error (RMSE), the mean absolute percentage error (MAPE), and the computational time of each model, as reported in Table 5.

According to Table 5, parameters I_0 and R_{sh} have the highest standard deviation, although the RMSE and the MAPE values are considerably low for the three models. This put into evidence the impact of the R_{sh} parameter in the zone near to I_{sc} , which is the beginning of the Q_2 zone. The low computation time of Bishop’s model supposes that the tuning parameters of GA are suitable for the number of parameters to estimate. In the case of SDM, computation time is higher since it has three times more iterations; a proper estimation of its parameters is a crucial task to ensure an accurate parameter estimation in Q_2 . The parameters of the DRM in reverse mode, and reported in Figure 4, were estimated following the instructions provided in [30]. First, it was necessary to identify the zones that could be linearized; in this case, the blue, red, and gray regions highlighted in Figure 6 are the zones to be linearized. Breakdown voltages V_{br1} , V_{br2} , and V_{br3} correspond to the points on the curve where the linear zone begins, i.e., 0 V, 2.318 V and 5.979 V, respectively.

The values of the resistors ($R_1 = 90 \Omega$, $R_2 = 40 \Omega$ and $R_3 = 26.31 \Omega$), which correspond to the slopes of the linear zones, were calculated through Ohm’s Law using the extreme points of the corresponding linear zone.

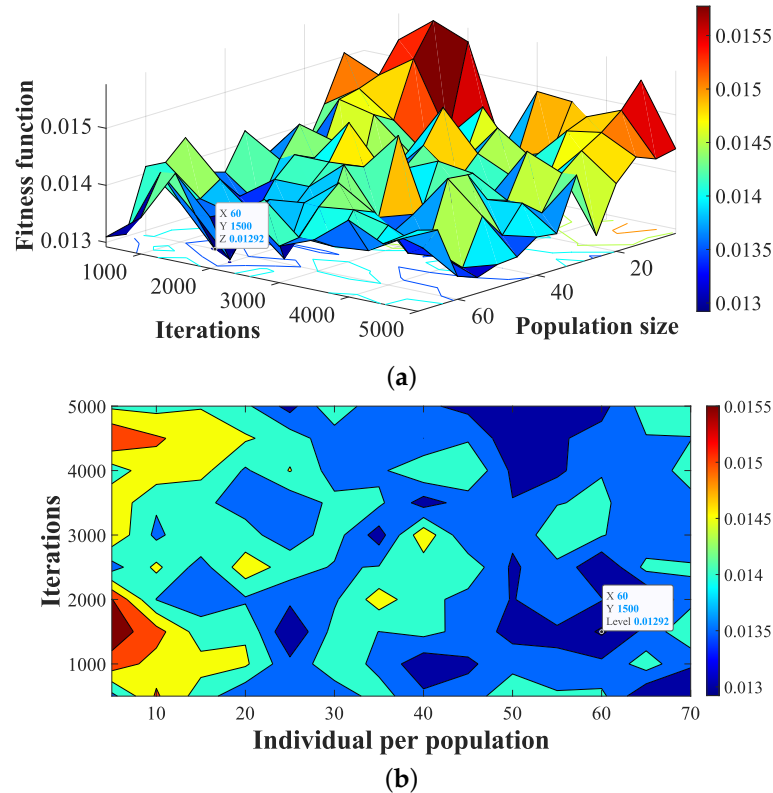


Figure 5. Selection of the estimation parameters for the SDM. (a) Mesh of fitness function in relation with the number of iterations and population size. (b) Contour of fitness function in relation with the number of iterations and population size.

Table 5. Parameters estimated for each model (mean \pm standard deviation).

Parameter	SDM	Bishop	DRM
I_{ph} [A]	0.431 ± 0.019	0.434 ± 0.0244	0.433 ± 0.025
I_0 [10^{-8} A]	5.665 ± 2.538	5.722 ± 2.538	5.118 ± 3.023
A	1.172 ± 0.065	1.361 ± 0.219	1.179 ± 0.081
R_s [Ω]	0.211 ± 0.086	0.619 ± 0.390	0.267 ± 0.124
R_{sh} [Ω]	47.409 ± 8.764	58.018 ± 16.597	59.877 ± 26.566
V_{br} [V]	-	-24.58 ± 9.15	-
m	-	-5.682 ± 1.774	-
a	-	0.016 ± 0.009	-
RMSE	0.022 ± 0.008	0.047 ± 0.017	0.032 ± 0.013
MAPE	0.155 ± 0.0940	0.3966 ± 0.1843	0.318 ± 0.169
Time [s]	49.803 ± 0.867	1.274 ± 0.601	3.123 ± 0.206

The circuit in Figure 4 was simulated in Simulink to obtain the I–V curve for the DRM. Then, an interpolation with the voltage vector of the experimental data was performed to compare the results of the cell current estimated by the DRM with that predicted by the SDM and the Bishop model.

Figure 7 illustrates the I–V curves obtained with each model using the best population function results taken from Table 6. In Q_1 , the three models show a high accuracy between simulation and experimental data. In Q_2 , the Bishop model provides the best result, while the SDM and the DRM exhibit a decrease in their accuracy.

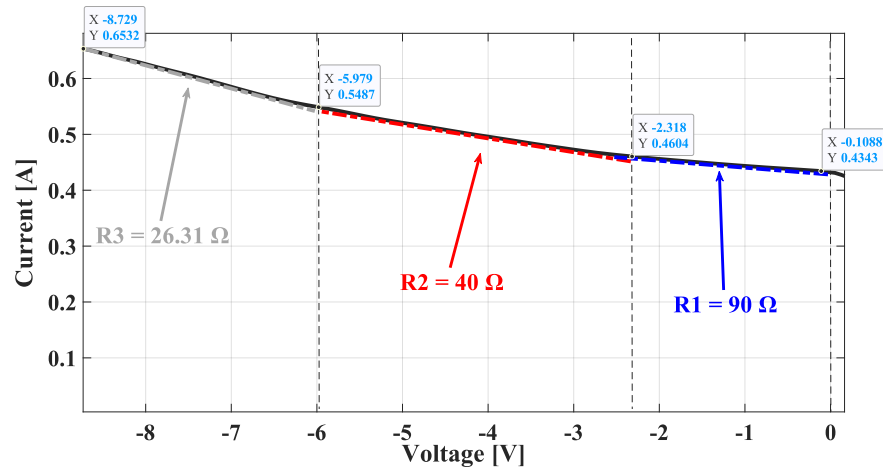


Figure 6. Estimation of DRM parameters for Q_2 .

The accuracy of the curve for the DRM depends on the linear zones chosen for the I–V characterization, as well as on the precise calculation of the number of branches. Moreover, the estimation of the parameters that define the DRM model in the first quadrant are the same ones used for the SDM, and those were estimated using only the information of the experimental I–V curve in the first quadrant. Finally, those parameters also affect the behavior of the models in the second quadrant (Q_2).

On the other hand, it is observed that the estimation provided by the SDM did not have a good approximation in Q_2 . This model presents a linear behavior for Q_2 , thus the breakdown voltage is not observed. Here, for the parametrization of this model, the whole information of the experimental I–V curve was used (Q_1 and Q_2).

Table 6. Parameters used for the best solution.

Parameter	SDM	Bishop	DRM
I_{ph} [A]	0.427	0.428	0.436
I_0 [10^{-8} A]	6.325	9.957	3.391
A	1.165	1.201	1.115
R_s [Ω]	0.157	0.179	0.117
R_{sh} [Ω]	41.825	63.900	86.443
V_{br} [V]	-	-23.31	-
m	-	-6.975	-
a	-	0.025	-

Table 7 presents the relative error of the main points of interest, i.e., I_{sc} , V_{oc} , I_{MPP} , and V_{MPP} . The three models show low error values, making them suitable for applications where the delivered power needs to be estimated [43].

As observed in Figure 8, the SDM and the Bishop model exhibit high accuracy for Q_1 representation, especially at the Maximum Power Point (MPP), which is the most relevant point for power analysis. For the DRM, there is a significant difference in the estimation of V_{oc} , while the estimation of I_{sc} exhibits a lower difference. However, both differences affect the estimated location of the maximum power point (MPP) in comparison with the one obtained in the experimental stage.

Figure 9 shows the power vs. voltage (P–V) curves near the MPP obtained with each model. Such curves were generated using the best population function results taken from Table 6. In this case, the Bishop model and SDM provide the best results for MPP estimation based on the experimental data. The Bishop model exhibits the smallest estimation error of 0.43%, while the error provided by SDM is 2.26%. On the other hand, the DRM presents an error of 4.01%, which is the highest deviation obtained.

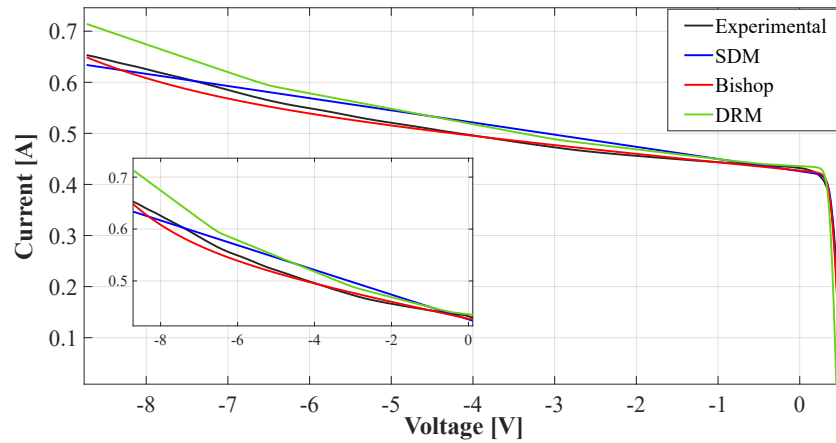


Figure 7. Comparison between the experimental and estimated curves in Q_1 and Q_2 (zoom-in for Q_2).

Table 7. Relative error of some points of interest in the I–V and P–V curves.

Parameter	SDM	Bishop	DRM
I_{sc} [A]	0.0415	0.007	0.0246
V_{oc} [V]	0.0795	7.91×10^{-4}	0.1526
I_{MPP} [A]	0.1316	0.0561	0.1422
V_{MPP} [V]	0	0.0207	0.1134

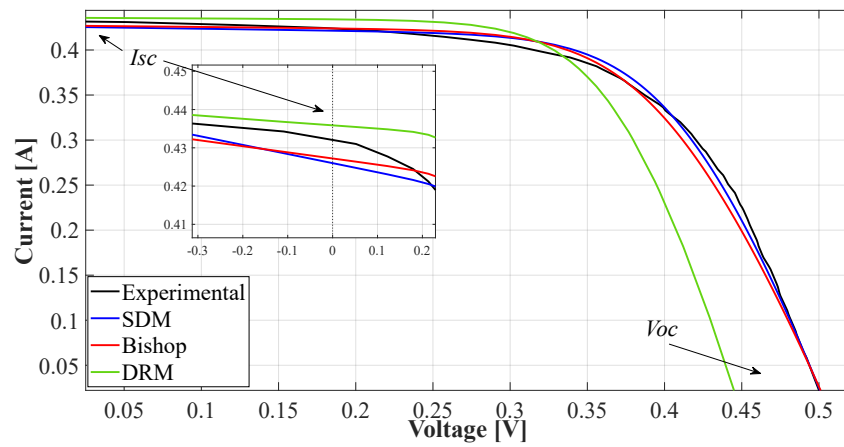


Figure 8. Comparison between the experimental and estimated curves (zoom-in for I_{sc}).

Finally, Figure 10 depicts the errors obtained for the best estimation of the SDM, the Bishop model, and the DRM. For Q_1 , the SDM provides the best result for I–V characterization, while for Q_2 the Bishop model exhibits the lowest error. In the case of the DRM, the I–V characterization depends on the accurate parameter estimation in Q_1 , highlighting the impact of R_{sh} as previously discussed.

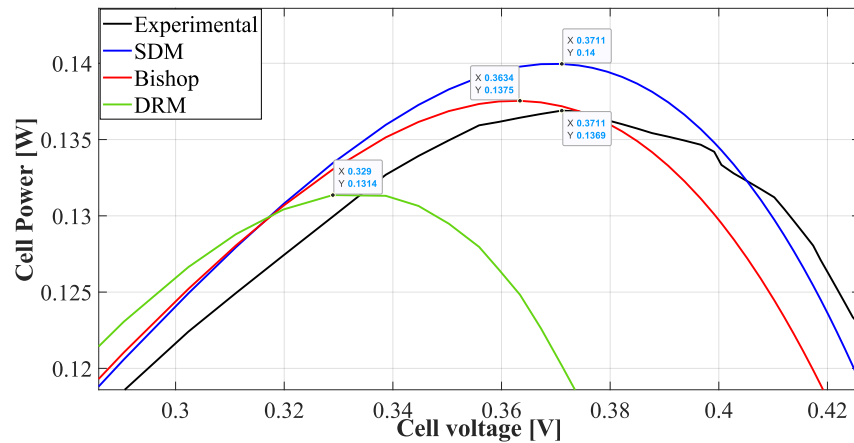


Figure 9. Maximum power point for each model .

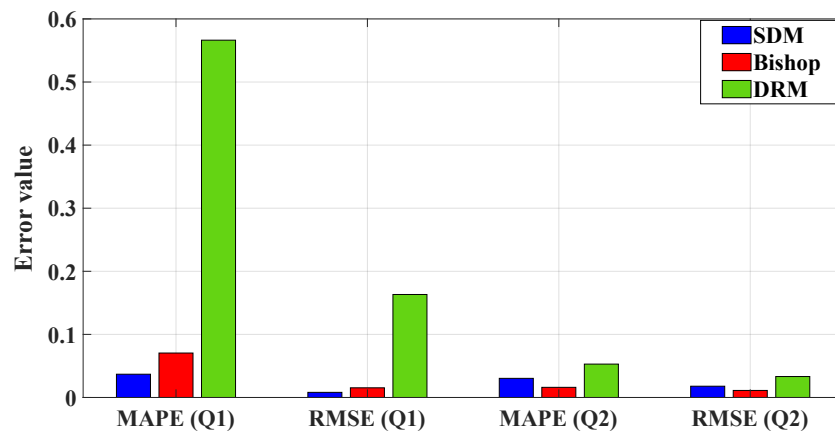


Figure 10. Estimation error for each model.

5. Conclusions

This paper presented a simple strategy for the I–V characterization of a PV cell considering three PV models. This proposed strategy uses GA and Simulink to extract the parameters from an experimental I–V curve. The analysis results demonstrate that the SDM model does not correctly reproduce the cell behavior when the current grows exponentially while the voltage at the cell terminals grows negatively (Q_2).

The parameter estimation of the DRM model, which was carried out in two stages, demonstrated that estimating the parameters per quadrant has a negative influence in the model accuracy. When estimating the parameters of the first quadrant, exclusively using the experimental information related to that quadrant, the critical parameter R_{sh} is not correctly identified, which is one of the parameters that imposes the behavior in the second quadrant. Moreover, the results reveal the need for a mathematical formulation that allows estimating the whole set of parameters of this particular model. Here, this procedure was developed with the circuital model evaluation in Simulink, which required the estimation of the five parameters for Q_1 described in Table 1 and the calculation of the parameters for Q_2 (see Figure 6), in an independent way.

It is also important to highlight that the proposed procedure can be used, along with PV array modeling methodologies, to analyze the behavior of cells operating in both Q_1 and Q_2 , which is needed for power analysis and losses estimation during partial shading conditions. Future works could consider estimating energy per day, month, or year using the electrical representation described for the PV cell modeling. Also, another future work

could consider to apply other optimization techniques to solve the parameter estimation problem, which may reduce both estimation errors and computation time.

Author Contributions: Conceptualization, B.J.R.-C., M.D.-F., L.A.T.-G. and C.A.R.-P.; methodology, B.J.R.-C., M.D.-F., L.A.T.-G. and C.A.R.-P.; software, B.J.R.-C.; validation, B.J.R.-C., M.D.-F., L.A.T.-G. and C.A.R.-P.; writing—original draft preparation, B.J.R.-C., M.D.-F. and L.A.T.-G.; writing—review and editing, B.J.R.-C., M.D.-F., L.A.T.-G. and C.A.R.-P. All authors have read and agreed to the published version of the manuscript.

Funding: The APC was funded by the Instituto Tecnológico Metropolitano (Dirección de investigaciones).

Institutional Review Board Statement: Not applicable.

Informed Consent Statement: Not applicable.

Data Availability Statement: The data used in this study are reported in the paper figures and tables.

Acknowledgments: Authors Bonie Restrepo and Luz Adriana Trejos thank the Instituto Tecnológico Metropolitano (PCI 20201 project) for supporting this research. Author Carlos Andres Ramos-Paja thanks to Universidad Nacional de Colombia (Hermes 51503 project) for supporting this research.

Conflicts of Interest: The authors declare no conflict of interest.

References

- IEA. Renewables 2020. 2020. Available online: <https://www.iea.org/reports/renewables-2020/solar-pv> (accessed on 15 September 2021).
- Abo-Sennah, M.; El-Dabah, M.; Mansour, A.E.B. Maximum power point tracking techniques for photovoltaic systems: A comparative study. *Int. J. Electr. Comput. Eng.* **2021**, *11*, 57–73. [[CrossRef](#)]
- Wen, Z.; Chen, J.; Cheng, X.; Niu, H.; Luo, X. A new and simple split series strings approach for adding bypass diodes in shingled cells modules to reduce shading loss. *Sol. Energy* **2019**, *184*, 497–507. [[CrossRef](#)]
- Jordehi, A.R. Parameter estimation of solar photovoltaic (PV) cells: A review. *Renew. Sustain. Energy Rev.* **2016**, *61*, 354–371. [[CrossRef](#)]
- Bradaschia, F.; Cavalcanti, M.C.; do Nascimento, A.J.; da Silva, E.A.; de Souza Azevedo, G.M. Parameter identification for PV modules based on an environment-dependent double-diode model. *IEEE J. Photovolt.* **2019**, *9*, 1388–1397. [[CrossRef](#)]
- Bishop, J. Computer simulation of the effects of electrical mismatches in photovoltaic cell interconnection circuits. *Sol. Cells* **1988**, *25*, 73–89. [[CrossRef](#)]
- Zegaoui, A.; Petit, P.; Aillerie, M.; Sawicki, J.P.; Charles, J.P. Experimental validation of photovoltaic direct and reverse mode model. Influence of partial shading. *Energy Procedia* **2012**, *18*, 1247–1253. [[CrossRef](#)]
- Gao, S.; Wang, K.; Tao, S.; Jin, T.; Dai, H.; Cheng, J. A state-of-the-art differential evolution algorithm for parameter estimation of solar photovoltaic models. *Energy Convers. Manag.* **2021**, *230*, 113784. [[CrossRef](#)]
- El-Fergany, A.A. Parameters identification of PV model using improved slime mould optimizer and Lambert W-function. *Energy Rep.* **2021**, *7*, 875–887. [[CrossRef](#)]
- Montano, J.; Tobón, A.; Villegas, J.; Durango, M. Grasshopper optimization algorithm for parameter estimation of photovoltaic modules based on the single diode model. *Int. J. Energy Environ. Eng.* **2020**, *11*, 367–375. [[CrossRef](#)]
- Huang, Y.C.; Huang, C.M.; Chen, S.J.; Yang, S.P. Optimization of module parameters for PV power estimation using a hybrid algorithm. *IEEE Trans. Sustain. Energy* **2019**, *11*, 2210–2219. [[CrossRef](#)]
- Alamri, H.R.; Rezk, H.; Abd-Elbary, H.; Ziedan, H.A.; Elnozahy, A. Experimental Investigation to Improve the Energy Efficiency of Solar PV Panels Using Hydrophobic SiO₂ Nanomaterial. *Coatings* **2020**, *10*, 503. [[CrossRef](#)]
- Liao, Z.; Chen, Z.; Li, S. Parameters extraction of photovoltaic models using triple-phase teaching-learning-based optimization. *IEEE Access* **2020**, *8*, 69937–69952. [[CrossRef](#)]
- Chen, X.; Yue, H.; Yu, K. Perturbed stochastic fractal search for solar PV parameter estimation. *Energy* **2019**, *189*, 116247. [[CrossRef](#)]
- Zhang, H.; Heidari, A.A.; Wang, M.; Zhang, L.; Chen, H.; Li, C. Orthogonal Nelder-Mead moth flame method for parameters identification of photovoltaic modules. *Energy Convers. Manag.* **2020**, *211*, 112764. [[CrossRef](#)]
- Shankar, N.; Saravanakumar, N. Solar photovoltaic module parameter estimation with an enhanced differential evolutionary algorithm using the manufacturer’s datasheet information. *Optik* **2020**, *224*, 165700.
- Montoya, O.D.; Ramírez-Vanegas, C.A.; Grisales-Norena, L.F. Parametric estimation in photovoltaic modules using the crow search algorithm. *Int. J. Electr. Comput. Eng.* **2022**, *12*, 82. [[CrossRef](#)]
- Mathew, D.; Rani, C.; Kumar, M.R.; Wang, Y.; Binns, R.; Busawon, K. Wind-driven optimization technique for estimation of solar photovoltaic parameters. *IEEE J. Photovolt.* **2017**, *8*, 248–256. [[CrossRef](#)]
- Hamid, N.; Abounacer, R.; Idali Oumhand, M.; Feddaoui, M.; Agliz, D. Parameters identification of photovoltaic solar cells and module using the genetic algorithm with convex combination crossover. *Int. J. Ambient. Energy* **2019**, *40*, 517–524. [[CrossRef](#)]

20. Kumar, M.; Shiva Krishna Rao K, D.V. Modelling and Parameter Estimation of Solar Cell using Genetic Algorithm. In Proceedings of the 2019 International Conference on Intelligent Computing and Control Systems (ICCS), Madurai, India, 15–17 May 2019; pp. 383–387. [\[CrossRef\]](#)
21. Tang, C.; Zhou, H. Inverse modelling of PV power prediction based on GA method. *IOP Conf. Ser. Earth Environ. Sci.* **2021**, *675*, 012080. [\[CrossRef\]](#)
22. Marinov, A.; Zahariev, S.; Ivanov, I.; Papanchev, T. Genetic algorithm for generation of PV panel curves from datasheets. In Proceedings of the 2021 17th Conference on Electrical Machines, Drives and Power Systems (ELMA), Sofia, Bulgaria, 1–4 July 2021; pp. 1–4.
23. Montano, J.J.; Noreña, L.F.G.; Tobon, A.F.; Montoya, D.G. Estimation of the parameters of the mathematical model of an equivalent diode of a photovoltaic panel using a continuous genetic algorithm. *IEEE Lat. Am. Trans.* **2022**, *20*, 616–623. [\[CrossRef\]](#)
24. Yang, Z.; Liao, K.; Chen, J.; Xia, L.; Luo, X. Output performance analysis and power optimization of different configurations half-cell modules under partial shading. *Optik* **2021**, *232*, 166499. [\[CrossRef\]](#)
25. Seapan, M.; Hishikawa, Y.; Yoshita, M.; Okajima, K. Detection of shading effect by using the current and voltage at maximum power point of crystalline silicon PV modules. *Sol. Energy* **2020**, *211*, 1365–1372. [\[CrossRef\]](#)
26. Mahammed, I.H.; Arab, A.H.; Bakelli, Y.; Khennene, M.; Oudjana, S.H.; Fezzani, A.; Zaghba, L. Outdoor study of partial shading effects on different PV modules technologies. *Energy Procedia* **2017**, *141*, 81–85. [\[CrossRef\]](#)
27. Zegaoui, A.; Boutoubat, M.; Sawicki, J.P.; Kessaissia, F.Z.; Djahbar, A.; Aillerie, M. Enhanced model of photovoltaic cell/panel/array considering the direct and reverse modes. *AIP Conf. Proc.* **2018**, *1968*, 030015.
28. Koffi, H.; Kuditcher, A.; Kakane, V.; Armah, E.; Yankson, A.; Amuzu, J. The Shockley five-parameter model of a solar cell: A short note. *Afr. J. Sci. Technol. Innov. Dev.* **2015**, *7*, 491–494. [\[CrossRef\]](#)
29. Boylestad, R.L.; Nashelsky, L. *Electronic Devices and Circuit Theory*; Pearson Educación: London, UK, 2002.
30. Zegaoui, A.; Petit, P.; Aillerie, M.; Sawicki, J.; Belarbi, A.; Krachai, M.; Charles, J. Photovoltaic cell/panel/array characterizations and modeling considering both reverse and direct modes. *Energy Procedia* **2011**, *6*, 695–703. [\[CrossRef\]](#)
31. Petit, P.; Zégaoui, A.; Aillerie, M.; Sawicki, J.P.; Charles, J.P. The Transistor based Direct and Reverse Mode model for photovoltaic strings and panels. *Energy Procedia* **2012**, *18*, 1240–1246. [\[CrossRef\]](#)
32. Ishaque, K.; Salam, Z. An improved modeling method to determine the model parameters of photovoltaic (PV) modules using differential evolution (DE). *Sol. Energy* **2011**, *85*, 2349–2359. [\[CrossRef\]](#)
33. Luo, X.; Cao, L.; Wang, L.; Zhao, Z.; Huang, C. Parameter identification of the photovoltaic cell model with a hybrid Jaya-NM algorithm. *Optik* **2018**, *171*, 200–203. [\[CrossRef\]](#)
34. Ghani, F.; Fernandez, E.; Almonacid, F.; O'Donovan, T. The numerical computation of lumped parameter values using the multi-dimensional Newton-Raphson method for the characterisation of a multi-junction CPV module using the five-parameter approach. *Sol. Energy* **2017**, *149*, 302–313. [\[CrossRef\]](#)
35. Jain, A.; Kapoor, A. Exact analytical solutions of the parameters of real solar cells using Lambert W-function. *Sol. Energy Mater. Sol. Cells* **2004**, *81*, 269–277. [\[CrossRef\]](#)
36. Premkumar, M.; Subramaniam, U.; Babu, T.S.; Elavarasan, R.M.; Mihet-Popa, L. Evaluation of mathematical model to characterize the performance of conventional and hybrid PV array topologies under static and dynamic shading patterns. *Energies* **2020**, *13*, 3216. [\[CrossRef\]](#)
37. Kang, T.; Yao, J.; Jin, M.; Yang, S.; Duong, T. A novel improved cuckoo search algorithm for parameter estimation of photovoltaic (PV) models. *Energies* **2018**, *11*, 1060. [\[CrossRef\]](#)
38. Jung, T.H.; Ko, J.W.; Kang, G.H.; Ahn, H.K. Output characteristics of PV module considering partially reverse biased conditions. *Sol. Energy* **2013**, *92*, 214–220. [\[CrossRef\]](#)
39. King, D.; Dudley, J.; Boyson, W. *PVSIM©: A Simulation Program for Photovoltaic Cells, Modules, and Arrays*; Technical Report; Sandia National Labs.: Albuquerque, NM, USA, 1996.
40. Quaschnig, V.; Hanitsch, R. Numerical simulation of current-voltage characteristics of photovoltaic systems with shaded solar cells. *Sol. Energy* **1996**, *56*, 513–520. [\[CrossRef\]](#)
41. Bastidas-Rodríguez, J.D.; Petrone, G.; Ramos-Paja, C.A.; Spagnuolo, G. A genetic algorithm for identifying the single diode model parameters of a photovoltaic panel. *Math. Comput. Simul.* **2017**, *131*, 38–54. [\[CrossRef\]](#)
42. Chin, V.J.; Salam, Z.; Ishaque, K. An accurate and fast computational algorithm for the two-diode model of PV module based on a hybrid method. *IEEE Trans. Ind. Electron.* **2017**, *64*, 6212–6222. [\[CrossRef\]](#)
43. Kumar, J.; Parhyar, N.R.; Panjwani, M.K.; Khan, D. Design and performance analysis of PV grid-tied system with energy storage system. *Int. J. Electr. Comput. Eng.* **2021**, *11*, 1077. [\[CrossRef\]](#)